Adsorption (2007) 13: 83–94
DOI 10.1007/s10450-007-9000-1

Adsorption kinetics of fluoride on iron(III)-zirconium(IV) hybrid oxide

Krishna Biswas · Durjoy Bandhoyapadhyay · Uday Chand Ghosh

Received: 14 April 2006 / Revised: 13 November 2006 / Accepted: 16 January 2007 / Published online: 7 April 2007

Abstract Fluoride occurs in some drinking water sources at levels that are hazardous to health. Tests were conducted to assess the ability of a mineral-based adsorbent to take-up fluoride ion. Consequently, in search of novel adsorbent media, crystalline and hydrous iron(III)-zirconium(IV) hybrid oxide (IZHO) was synthesized, and tested to determine its capacity and kinetics for fluoride adsorption. The Fourier Transform Infrared (FTIR) spectrum of IZHO indicated the presence of Fe–O–Zr linkage which showed hybrid nature of the synthetic oxide. The optimum pH range for fluoride adsorption was ranged between 4.0 and 7.0. The analyses of the isotherm equilibrium data using the Langmuir and the Redlich–Peterson model equations by linear and non-linear methods showed that the data fitted better with latter model than the former. Thermodynamic analysis showed spontaneous nature of fluoride adsorption, and that took place with the increase of entropy. The kinetic data obtained for fluoride adsorption on IZHO at pH 6.8 (± 0.1) and room temperature (303 ± 2 K) described both the pseudo-first order and the reversible first-order equations equally well ($r^2 = \sim 0.98$–0.99), and better than pseudo second order equation ($r^2 = \sim 0.96$–0.98) for higher concentrations (12.5 and 25.0 mg/dm^3) of fluoride. The kinetics of fluoride adsorption on the mixed oxide took place with boundary layer diffusion. External mass transport with intra-particle diffusion phenomena governed the rate limiting process, which has been confirmed from the Boyd poor non-linear kinetic plots.

Keywords Adsorption · Fluoride · Kinetics · Isotherm · Iron(III)-zirconium(IV) oxide

K. Biswas · D. Bandhoyapadhyay · U.C. Ghosh (✉)
Department of Chemistry, Presidency College, 86/1 College Street, Kolkata 700073, India
e-mail: ucg@vsnl.net

Abbreviations

C_i	The initial concentration (mg/dm^3) of fluoride in solution
C_e	The concentration of fluoride (mg/dm^3) in solution at equilibrium
C_a	The concentration of fluoride (mg/dm^3) in solution at any time, t
C_b	The concentration of fluoride in solid phase (mg/g) at any time, t
C_{a0}	The initial concentration of fluoride in solution (mg/dm^3)
C_{b0}	The initial concentration of fluoride in adsorbent phase (mg/g)
Cae	The equilibrium concentration of solute in solution (mg/dm^3)
q_e	The adsorption capacity (mg/g) at equilibrium
q_m	The monolayer adsorption capacity (mg/g)
q_t	The adsorption capacity (mg/g) at any time, t
B_{L}	The Langmuir adsorption equilibrium constant (dm^3/mg)
A_{L}	The Langmuir constant (dm^3/g)
A_{RP}	The Redlich–Peterson model isotherm constant (dm^3/g)
B_{RP}	The Redlich–Peterson model isotherm constant $(\mathrm{dm}^3/\mathrm{mg})^n_{\mathrm{RP}}$
n_{RP}	The Redlich–Peterson isotherm model exponent
k_1	The pseudo-first order rate constant (time^{-1})
k_2	The pseudo-second order rate constant (mg/g time)
t	time (min)
Xa	The fractional conversion of solute
$k^{\#}$	$(= k^1 + k^2)$ the overall rate constant (time^{-1})
k^1	The rate of forward reaction (time^{-1})
k^2	The rate of backward reaction (time^{-1})
k_B	$(= -k^{\#})$ the rate constant (time^{-1}) of Bhattacharya and Venkobachar model kinetics

R_L The equilibrium parameter
ΔG^0 The Gibbs free energy change (kJ/mol)
ΔH^0 The enthalpy change (kJ/mol)
ΔS^0 The entropy change (kJ/mol/K)
R The universal gas constant (8.314 J/mol/K)
T The absolute temperature (K)
D_f The film diffusion coefficient (cm^2/s)
D_p The pore diffusion coefficient (cm^2/s)
r_0 The mean radius (cm) of particles
k_i The diffusion rate constant ($mg/g\,min^{0.5}$)
F The fraction of solute adsorbed
Bt A mathematical function of F
C_L Liquid phase equilibrium concentration of adsorbate (mg/dm^3)
C_s Solid phase adsorbate concentration at equilibrium (mg/g)

1 Introduction

Fluoride is an essential mineral for the dental and bones health of mammals, but excessive intake of it through foods and drinks causes dental and or skeletal fluorosis which is the last stage of manifestation of fluoride toxicity. The permissible limit of fluoride in drinking water is 0.5 to 1.0 mg/dm^3. However, many countries globally have regions where underground aquifers used as only drinking water sources contain high fluoride (>1.5 mg/dm^3). The cause of high fluoride level in groundwater is geological. The fluoride minerals present in the vein of almost all rocks are fluorite (CaF_2) and fluoro-apatite [$3Ca_3(PO_4)_2$. CaF_2]. Mobilization of fluoride from that into ground water depends on the pH and residence time of percolated water through the beds of minerals. The presence of dissolved high bicarbonate in percolated water accelerates the release of fluoride from the minerals under the favorable geo-physical condition due to water-mineral interactions (Saxena and Ahmed 2001). The possible chemical reactions for dissolving excess fluoride in water percolates over the bed of fluoride minerals are:

$$CaF_2 + 2HCO_3^- \rightarrow CaCO_3 + 2F^- + H_2CO_3,$$

$$CaF_2 + H_2CO_3 + 2OH^- \rightarrow CaCO_3 + 2F^- + 2H_2O.$$

Additionally, fluoride contaminated water when percolates through the calcite ($CaCO_3$)-rich rock/soil converts to fluorite (CaF_2) mineral.

$$CaCO_3 + 2F^- + 2H^+ \rightarrow CaF_2 + H_2CO_3.$$

The freshly formed fluorite mineral contributes >8 mg F^- per dm^3 of water unless any other natural phenomena play any significant role for reducing fluoride level from percolated water.

The methods reported for reducing fluoride level from water are based on the principle of precipitation and surface adsorption. The precipitation of fluoride with lime and aluminum salts (Saha 1993; Hichour et al. 2000) was used to reduce fluoride level from industrial wastewater. Typically, lime reduces the fluoride concentration down to 10–20 mg/dm^3. The calcium ion (Ca^{2+}) released from the lime interacts with fluoride and form CaF_2 precipitate. The aluminum ion (Al^{3+}) released from the added aluminum salt interact with fluoride in water and form $AlF_x^{(3-x)+}$ and $Al(OH)_{(3-y)}F_y$ etc. This reduces fluoride concentration down to 2.0 mg/dm^3 (Yang and Dluhy 2002). This method, however, leads to the pH and dissolved solids value of treated water high, and results difficulty of eliminating excess chemicals (Castel et al. 2000).

Surface adsorption is another method, in which fluoride is adsorbed onto a membrane, or a fixed bed packed with resin or other material particles. Numerous techniques have been reported, such as reverse osmosis (Hichour et al. 1999; Pervov et al. 2000), limestone reactor (Reardon and Wang 2000) and activated alumina column (Wu 1978; Bishop and Sansoucy 1979). Among them, ion-exchange, eletrodyalysis and reverse osmosis are effective and can reduce the fluoride concentration to a suitable value, but expensive for third world countries.

In past ten years, many workers devoted their attention to develop low cost and effective adsorbent materials. A large number of materials have also been tested, such as alum sludge (Sujana et al. 1998), activated alumina (Tramfloc Inc 2005; Ghorai and Pant 2005), amorphous alumina (Li et al. 2001), metallurgical grade alumina (Pietrelli 2005), activated carbon (Srimurali et al. 1998), calcite (Yang et al. 1999), coal-based sorbent (Sivasamy et al. 2001), fly ash (Piekos and Paslawaska 1999), lanthanum impregnated silica gel (Wasay et al. 1996), red mud (Cengeloglu et al. 2002) and some low cost adsorbents (Fan et al. 2003; Jamode et al. 2004). Lab-bench scale removal of fluoride from contaminated water has been studied in our laboratory by using synthetic hydrous ferric oxide (Dey et al. 2004) and hydrous zirconium oxide (Goswami et al. 2004). Hydrous zirconium oxide showed greater fluoride adsorption capacity than hydrous ferric oxide.

Thus, the objective of the present work was to increase fluoride adsorption capacity of hydrous ferric oxide by adding low percentage of zirconium oxide. This paper concentrates on the synthesis of iron(III)-zirconium(IV) hybrid oxide (IZHO) adsorbent and that to apply for the studies of fluoride adsorption. As the adsorption kinetics guides the technologists for designing of continuous flow system, the kinetics on fluoride adsorption onto the synthetic hybrid oxide, herein, has been reported systematically.

2 Materials and methods

2.1 Reagents

Sodium fluoride (AR, BDH) was used for the preparation of the standard fluoride (1000 mg/dm^3) stock solution. Sodium 2-(para sulfophenyl azo)-1,8-dihydroxy-3,6-naphthalene disulfonate (SPADNS) and zirconyl oxychloride used for fluoride analysis were of GR (E. Merck) grade. Other chemicals used were of reagent grade.

2.2 Instruments

A pH-meter (Model: LI-127, ELICO India) was used for pH measurements throughout the experiments. UV-VIS spectrophotometer (Model: U3210, Hitachi Japan) was used for fluoride determination. X-ray diffraction (XRD) of the synthetic oxide was obtained from a Philips Mat, Holland, PW1730/10 diffractometer. Scanning Electron Microscopy (SEM) of the oxide was taken by using Cambridge-360 scanning electron microscope. Perkin Elmer-RXFT Spectrophotometer was used for Fourier Transform Infra Red (FTIR) analysis of the synthetic oxide. Simudza made thermal analyzer was used for thermal analysis of the synthetic oxide.

2.3 Iron(III)-zirconium(IV) mixed oxide synthesis

A mixture of 0.1 M Ferric chloride (in 0.01 M HCl) and 0.1 M zirconium oxychloride (in 0.01 M HCl) solutions (v/v = 9:1) was warmed at ∼80 °C, and hydrolyzed by drop wise addition of 0.1 M NaOH solution. The brown gel-like precipitate formed was aged with supernatant for 5 d at room temperature. The filtered precipitate was washed with water to remove chloride, and dried at 50–60 °C in an air oven. The dry product when treated with cold water converted into smaller particles. The particles ranged in 140–290 μm were used for the experiments.

2.4 Adsorption experiments

Batch adsorption experiments were conducted separately for evaluating the (i) effect of pH at 303 (±2) K for the concentrations 5.0, 12.5 and 25.0 mg F^-/dm^3 in the pH range 2.0 to 10.0, and (ii) isotherm equilibrium at pH 6.8 (±0.1) and at temperatures 283, 293 and 303 K in the concentration range 5.0 to 50.0 mg F^-/dm^3 by shaking (speed: 290 ± 10 rpm) the reaction mixture taken into 125 cm^3 capped polythene bottles. Here, 0.1 g of the mixed oxide (particle size: 140–290 μm) was thoroughly mixed with 50 cm^3 fluoride solutions. The pH of the solutions was adjusted with 0.1 M hydrochloric (HCl) and/or 0.1 M sodium hydroxide (NaOH), as required. Intermediate major pH change, if any, noted was controlled with above acid/alkali solution for determining optimum pH-range for fluoride adsorption.

The batch adsorption kinetic experiments were carried out by shaking (290 ± 10 rpm) 0.1 g of the mixed oxide with 50 cm^3 solution of the adsorbate (concentrations: 5.0, 12.5 and 25.0 mg F^-/dm^3) at a pH 6.8 (±0.1) and at a temperature 303 (±2) K. The reaction mixtures were taken into ten separate 125 cm^3 polythene bottles for each concentration. The major pH change, if any, noted during the run of experiment was adjusted using above acid or alkali solution, as required. The reaction mixtures with bottles were withdrawn regularly at a desired time interval, and filtered immediately using 0.45 μm membrane filters. The filtrates were analyzed for residual fluoride (Standard Methods 1998).

2.5 Theory

2.5.1 Equilibrium studies

The data of equilibrium isotherm studies are to be analyzed by the following two basic adsorption isotherm equations to understand the mechanism of heterogeneous reaction. This would provide some insight surface properties of the adsorbent and affinity for the adsorbate (see Table 1) where C_e and q_e are equilibrium concentration (mg/dm^3) of adsorbate species and adsorption capacity (mg/g) of adsorbent, respectively; A_L (dm^3/g) is the product of Langmuir equilibrium constant, B_L (dm^3/mg) and equilibrium adsorption capacity, q_m (mg/g). A_{RP} (dm^3/g) and B_{RP} (dm^3/mg) are the Redlich–Peterson model isotherm constants, respectively; n_{RP}, the Redlich–Peterson exponent, lies between 0 and 1. The Redlich–Peterson model isotherm converts to (i) the Langmuir model isotherm for $n_{RP} = 1$, (ii) the Freundlich isotherm model when A_{RP} and B_{RP} have value much greater than unity and (iii) the Henry's Law for $n_{RP} = 0$.

2.5.2 Adsorption kinetics

The adsorption kinetics analysis is an important aspect for evaluation of efficiency of an adsorption process. As the adsorption rate is very important for adsorption mechanism

Table 1

Isotherm	Nonlinear form	Equation number	Reference
Langmuir:	$q_e = (A_L C_e)/(1 + B_L C_e)$	(1)	Langmuir (1916)
Redlich–Peterson:	$q_e = (A_{RP} C_e)/(1 + B_{RP} C_e^n{}_{RP})$	(2)	Redlich and Peterson (1959)

and design of continuous flow system, the time-dependent adsorption data have analyzed by the following widely used kinetic equations:

Pseudo-first order equation (Lagergren 1898)

$$(dq_t/dt) = k_1(q_e - q_t) \tag{3}$$

where q_e and q_t are the adsorption capacities (mg/g) at equilibrium and at time t, respectively. k_1 is the rate constant of pseudo-first order adsorption reaction (time^{-1}). The integrated pseudo-first order rate equation at boundary conditions ($t = 0$ to $t = t$ and $q_t = 0$ to $q_t = q_t$) can be written as

$$\log(q_e - q_t) = \log q_e - k_1 t/2.303. \tag{4}$$

The plot of $\log(q_e - q_t)$ versus t should give a straight line from which the values for k_1 and q_e can be calculated from the slope and intercept of the plots, respectively.

Pseudo-second order equation The pseudo-second order adsorption kinetic rate equation is expressed as (Ho and McKay 1998):

$$(dq_t/dt) = k_2(q_e - q_t)^2 \tag{5}$$

where q_e and q_t have the same meaning mentioned above. k_2 is the rate constant for pseudo-second order adsorption reaction (g mg^{-1} time^{-1}). The integrated pseudo-second order rate equation at boundary conditions ($t = 0$ to $t = t$ and $q_t = 0$ to $q_t = q_t$) can be written as

$$1/(q_e - q_t) = 1/q_e + k_2 t. \tag{6}$$

Equation (6) can be rearranged to obtain the linear form:

$$t/q_t = 1/(k_2 q_e^2) + t/q_e \tag{7}$$

and

$$h = k_2 q_e^2 \tag{8}$$

where h is the initial adsorption rate (mg g^{-1} time^{-1}).

The straight line plots of t/q_t versus t for the kinetic data give the values for q_e and k_2 from the slope and intercept.

First-order reversible equation (Bhattarcharya and Venkobachar 1984) The kinetic model is based on a reversible reaction with equilibrium state being established between two phases, and can be written in the form as:

$$-(dC_a/dt) = (dC_b/dt) = C_a(dX_a/dt) = k^1 C_a - k^2 C_b = k^1(C_{a0} - C_{a0}X_a) - k^2(C_{b0} - C_a X_a) \tag{9}$$

where C_a (mg/dm^3) is the solute concentration in solution at any time, t and C_b (mg/g) the solute concentration on the adsorbent; C_{a0} and C_{b0} are the initial concentration of solute in solution and adsorbent, respectively. X_a is the fractional conversation of solute, and k^1 and k^2, respectively are the forward and backward first-order rate constants.

Applying the equilibrium conditions followed by integration and simplifying the above equation, it can be expressed as

$$-\ln[1 - U(t)] = k^{\#} t \tag{10}$$

where $U(t) = (C_{a0} - C_a)/(C_{a0} - C_{ae})$, C_{ae} is the equilibrium concentration of solute in solution, $k^{\#}$ $(= k^1 + k^2)$ the overall rate constant. Thus the above equation (10) becomes

$$\ln[1 - U(t)] = k_B t \quad (\text{where } k_B = -k^{\#}). \tag{11}$$

Therefore, the linear plots of $\ln[1 - U(t)]$ versus t give the value for k_B from the slope.

3 Results and discussion

3.1 Physicochemical characterization

The X-ray diffraction (XRD) pattern (Fig. 1) of iron(III)-zirconium(IV) hybrid oxide (IZHO) obtained between start and end angle (°2Θ), 10° and 80°, showed eighteen peaks, and most significant are at 35.33°, 26.9°, 56.14°, 11.56° and 39.45° with relative intensity >30%. The results indicated that IZHO is crystalline in nature. The scanning electron micrograph (SEM) image (Fig. 2) of IZHO showed the agglomerated surface morphology with irregular shape and porous nature, which indicates high surface area. The chemical composition of the oxide synthesized was analyzed and found the mole ratio of iron to zirconium 9:1, which is as per mole ratio added for synthesis. The isoelectric point (pH_{zpc}) determined for the oxide surface by pH titration is 7.1–7.2. The Fourier Transform Infrared (FTIR) spectrum (Fig. 3) for the synthetic oxide showed nine absorption bands at wave numbers (cm^{-1}) around 3754, 3393, 2926, 2367, 2075, 1619, 980, 676 and 485. The bands around 3754, 3393 and 1619 cm^{-1} are due to the stretching and bending modes of coordinated water and O–H bond, respectively. The sharp band at around 2367 cm^{-1} is for CO_2, which was presumably present in alkali used for synthesis of the mixed oxide. The weak band around 980 cm^{-1} is for Zr–O bond. The bands obtained at 676 and 485 cm^{-1} are the stretching and bending modes for Fe–O–Zr. As the band positions are shifted to higher and lower value compared to that of M–O in hydrous ferric oxide (671 and

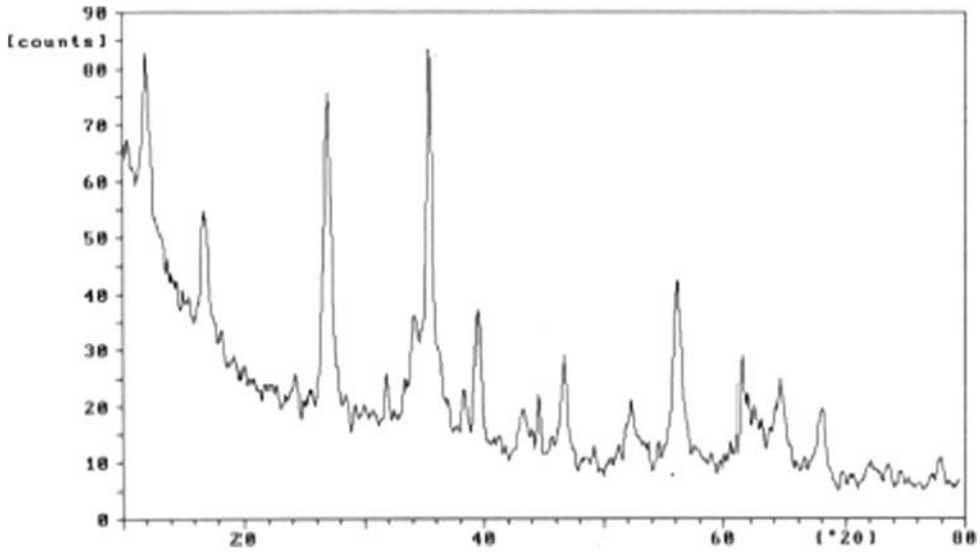

Fig. 1 X-ray diffraction pattern of IZHO

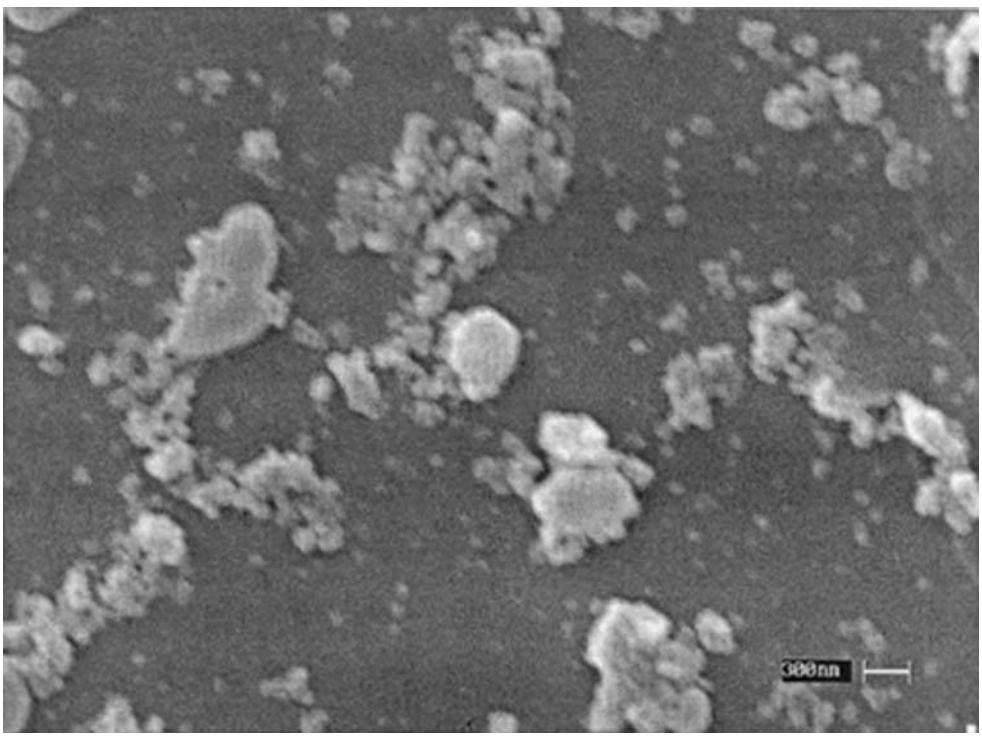

Fig. 2 Scanning electron micrograph (SEM) image of IZHO

461 cm^{-1}) indicated the formation of hybrid oxide. The extra two bands found at ∼2926 and ∼2075 cm^{-1} are presumably for stretching of symmetrical hydrogen bonded OH and the bending of lattice hole trapped OH, respectively. The two steps weight loss found in thermo gravimetric (TG) analysis, ∼16.7 and ∼11.4% at ∼100° and <200–600 °C, respectively correspond to physically adsorbed water and dehydroxylation from OH groups. The differential thermal (DT) analysis showed a sharp endothermic peak around 90–100 °C and a weak endothermic peak at >200–<300 °C, which correspond to the two steps weight loss. The results indicated the hydrous nature of the synthetic oxide.

3.2 Effect of pH

Figure 4 showed the results of fluoride adsorption on IZHO with varying pH at 303 (±2) K. The adsorption of fluoride from aqueous solution by IZHO increased with increasing solution pH from 2.0 to 4.0 and remained up to pH 7.0,

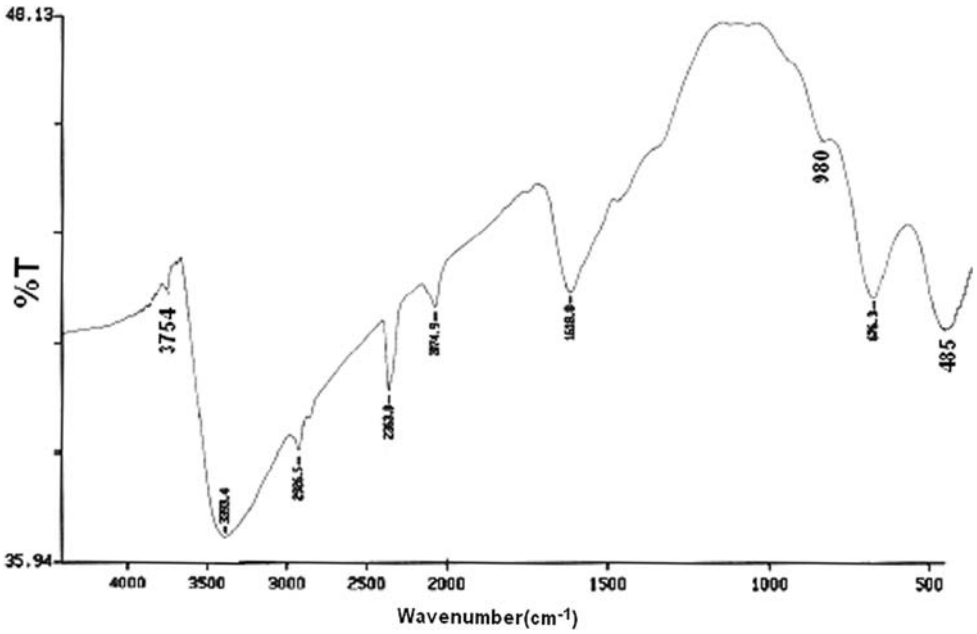

Fig. 3 Fourier Transform Infrared spectrum of IZHO

and decreased thereafter. In acid pH range, IZHO surface remains positive due to the reaction either (i) or (ii).

$$MOH + H_3O^+ \rightarrow MOH_2{}^+ + H_2O, \quad \text{(i)}$$

$$MOH + H_3O^+ \rightarrow M^+ + 2H_2O. \quad \text{(ii)}$$

Available fluoride ion in solution binds on the solid surface of the adsorbent with columbic forces, and results outer (iii) or inner sphere (iv) complex reaction. Less adsorption of fluoride in strong acid pH-range is due to (a) the equilibrium, $HF_{(aq)} \rightarrow H_{(aq)}{}^+ + F_{(aq)}{}^-$ shifts left for the common-ion effect, and effective available fluoride concentration for adsorption is lower than added ($pK_a^{HF} = 2.95$), and (b) the solubility loss of the adsorbent.

$$MOH_2{}^+ + F_{(aq)}{}^- \rightarrow MOH_2{}^+ - F^-, \quad \text{(iii)}$$

$$M^+ + F_{(aq)}{}^- \rightarrow M^+ - F^-. \quad \text{(iv)}$$

The increased adsorption of fluoride with increasing pH is due to the increase of available fluoride concentration in above dissociation reaction of HF and decrease in solubility of the oxide. However, the decreased fluoride adsorption on IZHO at pH > 7.0 is due to change of surface nature of the oxide. At pH > pH_{zpc} (7.1–7.2), the mixed oxide surface becomes negative; and the sodium ion (Na^+), available in solution with fluoride ion, adsorbs on negative surface sites of the solid (first sphere of adsorption) and fluoride ion adsorbs thereon (in secondary adsorption sphere) competing with OH^-.

$$MOH + Na^+ + F^- + OH^- \rightarrow MO^- - Na^+ - F^- + H_2O. \quad \text{(v)}$$

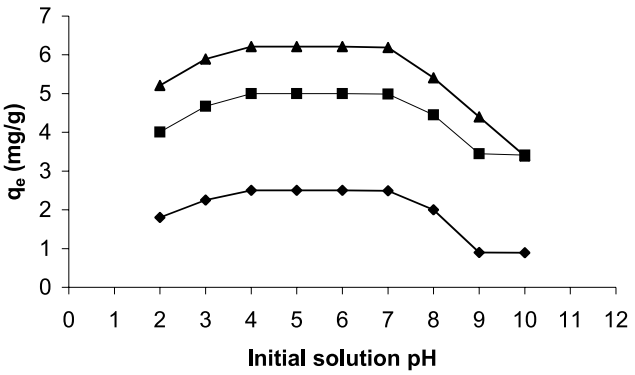

Fig. 4 Effect of initial pH on fluoride adsorption by IZHO at 303 K. Initial fluoride concentration (mg/dm^3) used: ♦ 5.0, ■ 12.5 and ▲ 25.0

The optimum pH range obtained for fluoride adsorption is 4.0 to 7.0. Thus, the remaining experiments were conducted at pH 6.8 (±0.1), which is typically a value in drinking water pH-range.

3.3 Adsorption isotherm

The equilibrium adsorption isotherm capacity (q_e, mg/g) determined for fluoride at pH 6.8 (±0.1), and at three different temperatures (283, 293 and 303 K) are shown as in Fig. 5 as data points against equilibrium fluoride solution concentration (C_e, mg/dm^3). As the isotherm analysis is important to know the equilibrium adsorption capacity and affinity of adsorbent, the experimental isotherm data shown (Fig. 5) have been analyzed separately by linear as well as non-linear methods for the Langmuir (see (1)) and the Redlich–Peterson (see (2)) isotherm model equations. The isotherm parameters obtained from linear and non-linear analyses are

Table 2 Linear isotherm parameters of fluoride adsorption on IZHO at pH 6.8 (±0.1)

Temperature (K)	Langmuir				Redlich–Peterson			
	A_L (dm^3/g)	q_m (mg/g)	B_L (dm^3/mg)	r^2	A_{RP} (dm^3/g)	B_{RP} (dm^3/mg)	n_{RP}	r^2
283	1.2113	7.50	0.1615	0.9886	1.44	0.260	0.920	0.9934
293	2.6983	7.51	0.3593	0.9909	3.75	0.669	0.921	0.9952
303	8.1903	8.21	0.9976	0.9986	16.16	2.606	0.922	0.9997

Table 3 Non-linear isotherm parameters of fluoride adsorption on IZHO at pH 6.8 (±0.1)

	Langmuir, $q_e = A_L C_e/(1 + B_L C_e)$					Redlich–Peterson, $q_e = A_{RP} C_e/(1 + B_{RP} C_e^{n_{RP}})$				
	A_L (dm^3/g)	B_L (dm^3/mg)	q_m (mg/g)	AAE*	AAPE** %	A_{RP} (dm^3/g)	B_{RP} $(dm^3/mg)^n_{RP}$	n_{RP}	AAE*	AAPE** %
283	1.2333	0.1655	7.454	0.254	6.891	3.7237	1.4253	0.7225	0.130	3.096
293	3.8641	0.5584	6.920	0.314	6.038	3.9609	1.8805	0.8511	0.234	5.950
303	54.5108	7.6520	7.124	0.619	10.971	152.454	28.3337	0.8875	0.369	8.596

AAE*: Average absolute error

AAPE**: Average absolute percent error

presented in Tables 2 and 3, respectively. The analysis of the parameters on the basis of r^2-value for linear method or on the basis of average absolute error (AAE) and average absolute percent error (AAPE) obtained for the non-linear fitting showed that the present data have fitted better with the Redlich–Peterson isotherm model equation (shown in Fig. 5) than the Langmuir, but the quality of the data fit became progressively somewhat poorer with increasing temperature. The value for the Redlich–Peterson exponent, n_{RP}, obtained is ranged from 0.72 to 0.89, and deviation from the unity indicating fewer tendencies to exhibit saturation behavior, as implied by the Langmuir isotherm. This is consistent with the lower quality of fit for the higher temperature. The increase of both the A_{RP} and A_L values with increasing temperature on the adsorption reaction indicates the increase of fluoride adsorption affinity of IZHO with rising temperature.

The equilibrium parameter R_L, which is defined as $R_L = 1/(1 + B_L C_i)$ where C_i is the initial concentration of adsorbate, was calculated in the concentration range (5–50.0 mg/dm^3) studied, and found the values lay in the range $0 < R_L < 1$. This indicated the fluoride adsorption on IZHO is favorable under the conditions of experiments.

The fluoride adsorption performance of IZHO at room temperature has been assessed by comparing the monolayer adsorption capacity (q_m, mg/g), though the value is temperature dependent, with some literature available data (Table 4). The results obtained showed that IZHO has greater affinity for fluoride than either of the reported data excepting metallurgical grade alumina. Though different forms of aluminum oxide have been studied for fluoride adsorption by

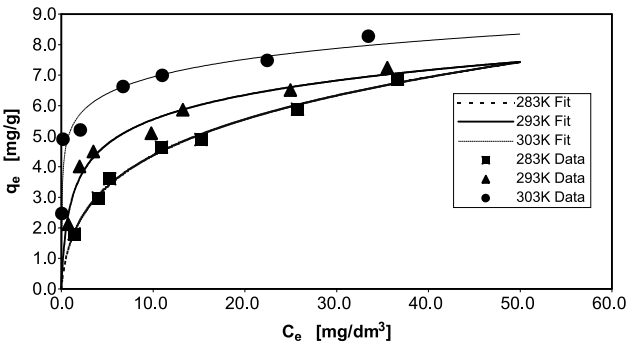

Fig. 5 Non-linear Redlich–Peterson isotherm (R-PI) plots for adsorption of fluoride at pH 6.8 (±0.1) on IZHO. Experimental data points at 303 K (♦), 293 K (▲), and 283 K (■); R-PI modeled fits: ····· (283 K), —— (293 K) and – – (303 K)

different authors and showed different efficiency, the trace solubility of aluminum as fluorocomplex might occur and long term drinking of such water is presumably the root of increasing Alzheimer's disease, a neurological problem, for the persons especially those who have poor kidney function. In this light the present adsorbent has promising prospect in this area.

3.4 Thermodynamics parameters

Thermodynamics parameters such as the changes of Gibbs free energy (ΔG^0), enthalpy (ΔH^0) and entropy (ΔS^0) for the adsorption of fluoride on IZHO are calculated by using

Table 4 A comparative assessment on fluoride adsorption performance of IZHO with some literature available data

Adsorbent	q_m^*, mg/g	Reference
Metallurgical grade alumina	12.57	Pietrelli (2005)
Active alumina	7.08	
Alum sludge	5.394	Sujana et al. (1998)
Hydroxyapatite	4.54	Fan et al. (2003)
Fluorspar	1.79	
Activated quartz	1.16	
Calcite	0.39	
Quartz	0.19	
Activated alumina	2.41	Ghorai and Pant (2005)
Lignite	7.09	Sivasamy et al. (2001)
Bituminous coal	7.44	
Iron-Zirconium Hybrid Oxide (IZHO)	8.21	Present work
Hydrous ferric oxide	7.50	Estimated by the authors under same conditions of present work
Hydrous zirconium oxide	10.21	Estimated by the authors under same conditions of present work

q_m^* value is compared taking the value obtained from the linear analysis of Langmuir model as other values shown are given from the analysis of same model

(12) to (14).

$$\Delta G^0 = -2.303RT \log_{10} B_L, \tag{12}$$

$$\log_{10} B_L(T_2) - \log_{10} B_L(T_1) = -(\Delta H^0/2.303R)[1/T_2 - 1/T_1], \tag{13}$$

$$\Delta S^0 = (\Delta H^0 - \Delta G^0)/T \tag{14}$$

where R is the universal gas constant (8.314 J/mol/K), T is the absolute temperature (K) and B_L is the Langmuir equilibrium constant.

The Gibbs free energy change values (kJ/mol) calculated using the Langmuir equilibrium constant (B_L), obtained by linear analysis, are –21.51 and –24.81, respectively at 293 and 303 K. The Gibbs free energy change values obtained for the adsorption of fluoride on IZHO indicated the adsorption process is spontaneous in nature, and the spontaneity of adsorption reaction increases with increasing temperature. Again, the high positive ΔH^0 value (+65.04 kJ/mol) calculated indicates the adsorption of fluoride onto the IZHO is endothermic. The calculated positive ΔS^0 value (+0.2962 kJ/mol/K) indicates the increase in entropy indicating the adsorption phenomenon takes places with increasing number of molecules/ions at solid-liquid interface. This is presumably due to the increase in solvent molecule at the solid-liquid interface because when hydrated fluoride ion adsorbs onto the solid surface, the water molecules released at the solid-liquid interfacial position which is greater in moles than the fluoride ions being adsorbed by the solid.

3.5 Adsorption kinetics

The time dependent fluoride adsorption data on IZHO at room temperature (303 ± 2) K are shown in Fig. 6 which shows that ≥90% of adsorbed fluoride took place in 45 min of contact, and the adsorption reaction was taken ~60 min for reaching equilibrium at the concentration range (5.0–25.0 mg/dm^3) studied. However, the equilibrium time required for adsorption of fluoride from 5.0 mg F^-/dm^3 solution was ~45 min, and that increased with increasing initial fluoride concentration; but the rapid adsorption was noted with increasing load of adsorbate in solution. Thus, the higher equilibrium time required for adsorption of fluoride with increasing concentration is presumably due to (i) the increase of columbic repulsion between adsorbed fluoride ions and the fluoride ions approaching the solid for adsorption from the solid-liquid interface, and (ii) slow intra-particle diffusion which is concentration gradient dependent.

The present adsorption data were analyzed by using pseudo-first order (see (4)), pseudo-second order (see (7)) and reversible first order (see (11)) kinetic equations. The kinetic parameters calculated from the slope and intercept of linear plots (Figs. 7, 8, 9) are shown in Table 5. The present kinetic data for fluoride adsorption on IZHO are described better by both the pseudo-first order and reversible first-order equations (r^2 = ~0.99 and ~0.98) than the pseudo-second order equation (r^2 = ~0.98 and ~0.96) for the studied higher two concentrations (12.5 and 25.0 mg/dm^3) of fluoride. However, the kinetic data obtained for 5.0 mg/dm^3 of fluoride solution are better described by the pseudo-

Table 5 Kinetics parameters for fluoride adsorption on IZHO at pH 6.8 (±0.1) and at temperature 303 (±2) K

Fluoride concentra-ion (mg/dm^3)	Pseudo-first order			Pseudo-second order				Reversible first order	
	$k_1 \times 10^{-2}$ min^{-1}	q_e mg/g	r^2	$k_2 \times 10^{-2}$ g/(mg min)	$h \times 10^{-2}$ mg/(g min)	q_e mg/g	r^2	$k_B \times 10^{-2}$ min^{-1}	r^2
5.0	5.06	2.12	0.9786	3.37	26.23	2.79	0.9867	5.09	0.9784
12.5	5.25	4.21	0.9923	2.60	82.41	5.63	0.9835	5.25	0.9924
25.0	4.47	5.64	0.9767	1.77	88.99	7.09	0.9608	4.45	0.9763

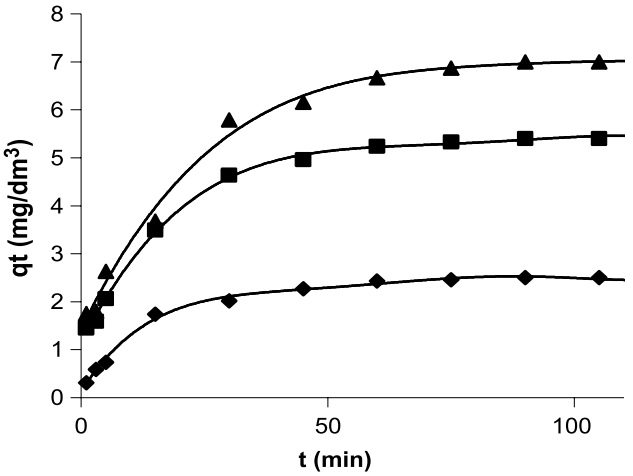

Fig. 6 Kinetic data for fluoride adsorption on IZHO at 303 (±2) K and pH 6.8 (±0.1). Initial fluoride concentration (mg/dm^3) used: ♦ 5.0, ■ 12.5 and ▲ 25.0

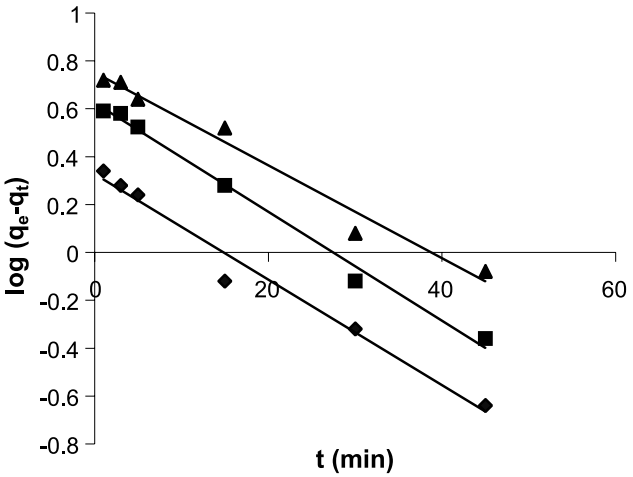

Fig. 7 Pseudo-first order kinetic plot for fluoride adsorption data on IZHO at 303 (±2) K and at pH 6.8 (±0.1). Initial fluoride concentration (mg/dm^3) used: ♦ 5.0, ■ 12.5 and ▲ 25.0

second order equation ($r^2 = \sim 0.99$) than the other two equations ($r^2 = \sim 0.98$). Thus, the orders, based on r^2, obtained to describe the kinetics of fluoride adsorption are:

Pseudo-second order > pseudo-first order ≈ reversible first order for 5.0 mg/dm^3, and pseudo-first order ≈ reversible first order > pseudo-second order for 12.5 and 25.0 mg/dm^3 of fluoride solutions. The other two kinetic model equations frequently used by some authors viz. power function ($\log q_t = \log a + b \log t$) and simple Elovich ($q_t = a + 2.303b \log t$), are also used to analyze the present data (plots not shown). The linear regression coefficient (r^2) values obtained reveal that both the power function and the simple Elovich equations explain the present kinetic data less well ($r^2 = 0.94$ to 0.98 for power function and 0.89 to 0.96 for simple Elovich equations) compared to the used other three equations. However, the data described both the power function and Elovich equations increasingly well with decreasing fluoride concentration in solution.

Fig. 8 Pseudo-second order kinetic plot for fluoride adsorption data on IZHO at 303 (±2) K and at pH 6.8 (±0.1). Initial fluoride concentration (mg/dm^3) used: ♦ 5.0, ■ 12.5 and ▲ 25.0

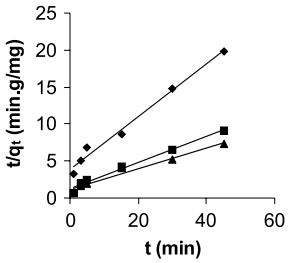

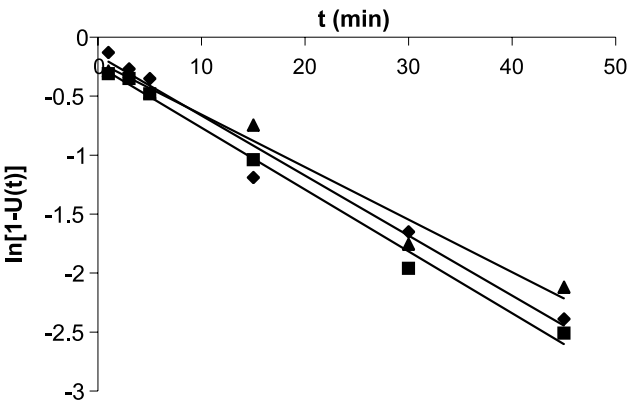

Fig. 9 Reversible first order kinetic plot for fluoride adsorption data on IZHO at 303 (±2) K and at pH 6.8 (±0.1). Initial fluoride concentration (mg/dm^3) used: ♦ 5.0, ■ 12.5 and ▲ 25.0

3.6 Film and intra particle diffusion

In order to asses the nature of the diffusion process responsible for adsorption of fluoride on the IZHO, attempts were made to calculate the coefficients of the process. If film diffusion is to be the rate determining step in the present adsorption kinetic study, the value of film diffusion coefficient (D_f) should be in the range 10^{-6} to 10^{-8} cm^2/s. If pore diffusion is to be the rate limiting, the pore diffusion coefficient (D_p) should be in the range 10^{-11}–10^{-13} cm^2/s (Michelson et al. 1975). Assuming spherical geometry for the adsorbent particles, the overall rate constant of the process can be correlated with the film diffusion coefficient and pore diffusion coefficient independently in accordance with the expressions (Bhattarcharya and Venkobachar 1984).

$$\text{Pore diffusion coefficient} \quad (D_p) = 0.03(r_0^2/t_{1/2}),$$

$$\text{Film diffusion coefficient} \quad (D_f) = 0.23(r_0 \partial C_S/t_{1/2}C_L),$$

where r_0 is the mean radius of the adsorbent particles (1.125×10^{-2} cm), ∂ is the film thickness (10^{-3} cm) (Helferich 1962), C_S and C_L are the concentrations of adsorbate in solid and liquid phase at $t = t$ and $t = 0$, respectively; and $t_{1/2}$ is time required for 50% adsorption. Inserting calculated $t_{1/2}$ value from the appropriate reaction kinetic equation and other appropriate present data, the film and pore diffusion coefficients were calculated (Table 6) for studied three different concentrations of fluoride in solution. The calculated D_f-values, (0.8 to 3.6) $\times 10^{-9}$ cm^2/s, are found to be lesser than 10^{-8} cm^2/s, and the D_p-values (10^{-8} to 10^{-9} cm^2/s) are clearly higher than 10^{-11} cm^2/s. Thus, it could be suggested that the adsorption kinetics of the present reaction is controlled mainly by film (boundary layer) diffusion with some possibility of intra-particle transport, as D_f-values obtained are in between 10^{-8} and 10^{-11} cm^2/s. This is confirmed from the plots of the experimental data according to

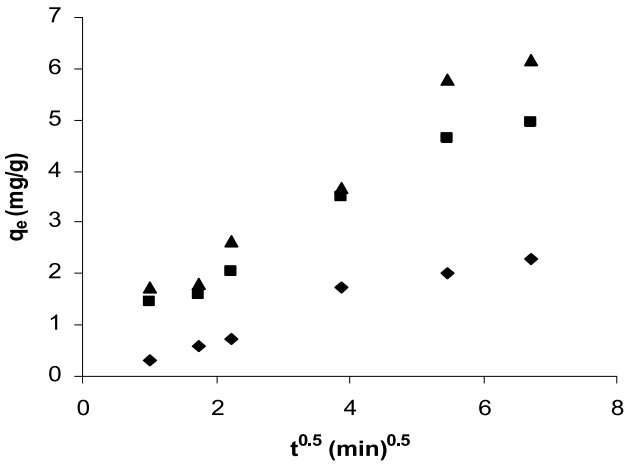

Fig. 10 q_t versus $t^{0.5}$ plot for fluoride adsorption data on IZHO at 303 (±2) K and at pH 6.8 (±0.1). Initial fluoride concentration (mg/dm^3) used: ♦ 5.0, ■ 12.5 and ▲ 25.0

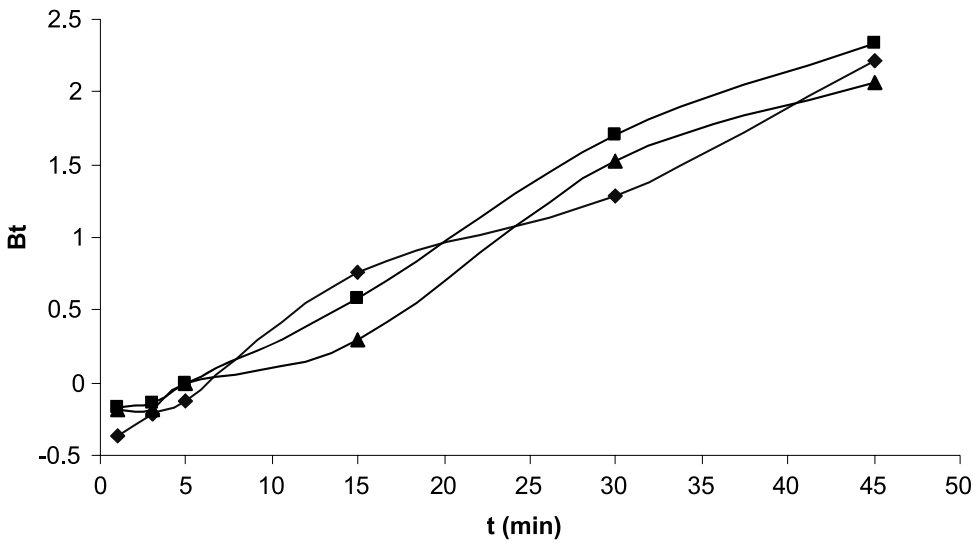

Fig. 11 Boyd kinetic plots on the adsorption of fluoride on IZHO at pH 6.8 (±0.1) and at 303 (±2) K. Initial fluoride concentration (mg/dm^3) used: ♦ 5.0, ■ 12.5 and ▲ 25.0

Table 6 Diffusion coefficients of fluoride removal on the IZHO

Fluoride concentration (mg/dm^3)	Film diffusion coefficient, D_f (cm^2/s)	Pore diffusion coefficient, D_p (cm^2/s)
5.0	3.66×10^{-9}	1.05×10^{-8}
12.5	1.40×10^{-9}	4.79×10^{-9}
25.0	0.8×10^{-9}	4.08×10^{-9}

the intra-particle diffusion model which is defined as follows:

$$q_t = k_i(t^{0.5}) \tag{15}$$

where the parameter, k_i (mg/g min$^{0.5}$), is the diffusion rate constant. In theory the plot between q_t and $t^{0.5}$ is given by multiple regions representing the external mass transfer followed by intra-particle diffusion in macro, meso, and micro pores (Kumar et al. 2005). The Fig. 10, the plot of q_t versus $t^{0.5}$ indicated two linear portions which suggest clearly two stage diffusion of fluoride onto the IZHO at studied highest concentration. The slope of the second linear portion characteristics the rate parameter corresponding to the intra-particle diffusion, whereas the intercept of this second linear portion is proportional to the boundary layer thickness.

3.7 Boyd kinetics

In order to determine the actual rate-controlling step involved in the fluoride adsorption process, the adsorption data were further analyzed using the kinetic expression developed by Boyd et al. (Kumar et al. 2005; Gupta and Ali 2001)

$$F = 1 - (6/\pi^2)\exp(-Bt) \tag{16}$$

where $F(= q_t/q_e)$ is the fraction of solute adsorbed at different times t and Bt is a mathematical function of F. q_t and q_e are the amount adsorbed (mg/g) at any time t and at equilibrium. Simplifying (16), the kinetic expression becomes

$$Bt = -0.4985 - \ln(1 - q_t/q_e). \tag{17}$$

Taking measured q_e and q_t, the Bt values are calculated from (17) for each value of F, and plotted against time as shown in Fig. 11. The poor non-linearity of Boyd plots (Fig. 11) indicated the external mass transport with intra-particle diffusion controlled the rate-limiting process of adsorption, which is different from the conclusion drawn by Wang and Li (2005) on adsorption of dye on unburned carbon.

4 Conclusion

The synthetic IZHO was crystalline and of hydrous nature. The optimum pH range where fluoride adsorption was good is between 4.0 and 7.0. Both linear and non-linear analyses showed the present isotherm equilibrium data fit is better with the Redlich–Peterson model than the Langmuir model, and the goodness of fit decreased with increasing temperature for non-linear analysis. The adsorption of fluoride on to the solid was spontaneous, and took place with the increase of entropy. The kinetic data for fluoride adsorption on IZHO obtained at 303 (±2) K described both the pseudo-first order and the reversible first-order equations equally good with correlation coefficient value (∼0.98–0.99) for higher two concentrations while those described the pseudo-second order equation better ($r^2 > 0.98$) than former two equations for 5.0 mg/dm^3 of fluoride. However, the same kinetic data described the other tested kinetic equations less well ($r^2 = 0.94$ to 0.98 for the power function and 0.89 to 0.96 for the simple Elovich equations) compared to the other three used equations. The kinetics of fluoride adsorption on the mixed oxide was found to take place not so clearly with boundary layer diffusion. External mass transport with intra-particle diffusion phenomena controlled the rate limiting process, which has been confirmed from Boyd poor non-linear kinetic plot.

Acknowledgements The authors acknowledged gratefully to the Ministry of Water Resources and Central Ground Water Board, New Delhi (India) for financial support and fellowship to one of the author (KB). The authors are also grateful to the Head, Department of Chemistry and the Principal, Presidency College, Kolkata for laboratory facilities.

References

Bhattarcharya, A.K., Venkobachar, C.: Removal of cadmium(II) by low costadsorbents. J. Environ. Eng. Div. ASCE Proc. **110**, 110–122 (1984)

Bishop, P.L., Sansoucy, G.: Fluoride removal from drinking water by activated alumina. J. Am. Water Works Assoc. **71**, 554–561 (1979)

Castel, C., Schweizer, M., Simonnot, M.O., Sardin, M.: Selective removal of fluoride ions by a two-way ion-exchange cyclic process. Chem. Eng. Sci. **55**, 3341–3352 (2000)

Cengeloglu, Y., Kir, E., Ersoz, M.: Removal of fluoride from aqueous solution by using red mud. Sep. Purif. Technol. **28**, 81–86 (2002)

Dey, S., Goswami, S., Ghosh, U.C.: Hydrous ferric oxide (HFO)—a scavenger for fluoride from contaminated water. Water Air Soil Pollut. **158**, 311–323 (2004)

Fan, X., Parker, D.J., Smith, M.D.: Adsorption kinetics of fluoride on low cost materials. Water Res. **37**, 4929—4937 (2003)

Ghorai, S., Pant, K.K.: Equilibrium, kinetics and breakthrough studies for adsorption of fluoride on activated alumina. Sep. Purif. Technol. **42**(3), 265–271 (2005)

Goswami, S., Dey, S., Ghosh, U.C.: Studies on removal of fluoride by hydrated zirconium oxide (HZO). Chem. Environ. Res. **13**, 117–126 (2004)

Gupta, V.K., Ali, I.: Removal of DDD and DDE from wastewater using bagasse fly ash, a sugar industry waste. Water Res. **35**, 33–40 (2001)

Helfferich, F.: Ion-Exchange. McGraw–Hill, New York (1962)

Hichour, M., Persin, F., Molenat, J., Sandeaux, J., Gavach, C.: Desalination **122**, 53–62 (1999)

Hichour, M., Persin, F., Sandeaux, J., Gavach, C.: Fluoride removal from waters by Donnan dialysis. Sep. Purif. Technol. **18**, 1–11 (2000)

Ho, Y.S., McKay, G.: Sorption of dye from aqueous solution by peat. Chem. Eng. J. **70**, 115–124 (1998)

Jamode, A.V., Sapkal, V.S., Jamode, V.S.: Defluoridation of water using inexpensive adsorbents. J. Ind. Inst. Sci. **84**, 163–171 (2004)

Kumar, V.K., Ramamurthi, V., Sivanesan, S.: Modeling the mechanism involved during the sorption of methylene blue onto fly ash. J. Colloid Interface Sci. **284**, 14–21 (2005)

Lagergren, S.: Zur Theorie der sogenannten adsorption gelöster stoffe. Kungliga Svenska Vetenskapsakademiens. Handlingar **24**(4), 1–39 (1898)

Langmuir, I.: The constitution and fundamental properties of solids and liquids. J. Am. Chem. Soc. **38**, 2221–2295 (1916)

Li, Y.H., Wang, S., Cao, A., Zhao, D., Zhang, X., Xu, C., Luan, Z., Ruan, D., Liang, J., Wu, D., Wei, B.: Adsorption of fluoride from water by amorphous alumina supported on carbon nanotube. Chem. Phys. Lett. **350**, 412–416 (2001)

Michelson, L.D., Gideon, P.G., Pace, E.G., Kutal, L.H.: Removal of soluble mercury from wastewater by complexing techniques. Bull No. 74, US Dept. Industry, Office of Water Research and Technology (1975)

Pervov, A.G., Dudkin, E.V., Sidorenko, O.A., Antipov, V.V., Khakhnov, S.A., Makarov, R.I.: RO and RF membrane systems for drinking water production and their maintenance techniques. Desalination **132**, 315–321 (2000)

Piekos, R., Paslawaska, S.: Fluoride uptake characteristics of fly ash. Fluoride **32**, 14–19 (1999)

Pietrelli, L.: Fluoride wastewater treatment by adsorption onto Metallurgical grade alumina. Ann. Chim. **95**(5), 303–312 (2005)

Reardon, E.J., Wang, Y.: Limestone reactor for fluoride removal from wastewaters. Environ. Sci. Technol. **34**(15), 3247–3253 (2000)

Redlich, O., Peterson, D.L.: A useful adsorption isotherm. J. Phys. Chem. **63**, 1024 (1959)

Saha, S.: Treatment of aqueous effluent for fluoride removal. Water Res. **27**, 1347–1350 (1993)

Saxena, V.K., Ahmed, S.: Dissolution of fluoride in groundwater: a water-rock interaction study. Environ. Geol. **40**, 1084–1087 (2001)

Sivasamy, A., Singh, K.P., Mohan, D., Muruthamuthu: Studies on defluoridationof water by coal-based sorbents. J. Chem. Tech. Biotech. **76**, 717–722 (2001)

Srimurali, M., Pragathi, A., Karthikeyan, J.: A study on removal of fluorides from drinking water by adsorption onto low cost materials. Environ. Pollut. **99**, 285—289 (1998)

Standard Methods for the Examination of Water and Wastewater, 20th edn. AWWA/APHA/WEF, Washington (1998)

Sujana, M.G., Thakur, R.S., Rao, S.B.: Removal of fluoride from aqueous solution by using alum sludge. J. Colloid Interface Sci. **206**(1), 94–101 (1998)

Tramfloc, Inc.: Fluoride removal by activated alumina. PO Box 350, Tempe, AZ 85280–0350, water@tramfloc.com, copyright© 1997–2005, Tramfloc, Inc. (2005)

Wang, S., Li, H.: Kinetic modelling and mechanism of dye adsorption of dye adsorption on unburned carbon. Dyes Pigments. Available online at www.sciencedirect.com (2005)

Wasay, S.A., Haron, Md.J., Tokunaga, S.: Adsorption of fluoride, phosphate and arsenate ions on lanthanum impregnated silica gel. Water Environ. Res. **68**, 295–300 (1996)

Wu, Y.C.: Activated alumina removes fluoride from water. J. Water Sew. Works **125**, 76–87 (1978)

Yang, C.L., Dluhy, R.: Electrochemical generation of aluminium sorbent for fluoride adsorption. J. Hazard. Mater. **94**(3), 223–238 (2002)

Yang, M., Hashimoto, T., Hoshi, N., Myoga, H.: Fluoride removal in a fixed bed packed with granular calcite. Water Res. **33**(16), 3395–3402 (1999)